Development of Numerical Models to Investigate Permeability Changes and Gas Emission around Longwall Mining Panel

Esterhuizen, G.S.
NIOSH, Pittsburgh Research Laboratory, Pittsburgh, Pennsylvania, USA

Karacan, C.O.
NIOSH, Pittsburgh Research Laboratory, Pittsburgh, Pennsylvania, USA

ABSTRACT: Underground longwall mining of coal causes large scale disturbance of the surrounding rock mass. The disturbance can increase the rock mass permeability through a reduction on the stress as well as formation of new fractures in the rock. Methane gas contained in the disturbed rock mass can migrate towards the low pressure mine workings and present an explosion hazard. This paper describes the application of a finite difference program to develop a geomechanical model that predicts permeability changes within the rock mass. The calculated permeabilities are used as input to a reservoir simulator that models methane desorption from the coal matrix, methane release from the rock layers and flow towards the mine excavations. The model also considers the basic characteristics of the mine ventilation network.

The geomechanical model uses empirical relationships between fracture permeability and stress to calculate permeability changes around a longwall face. The extent of rock failure is determined using a strain softening model that considers both rock matrix and bedding plane failure. The cave rock (gob) is modeled as a compressible, granulated material. The calculated horizontal and vertical permeabilities around the longwall face are averaged and used as one of the inputs to the reservoir model. The reservoir model was developed and calibrated against records of methane flow at a study mine in southwestern Pennsylvania. Good correlation between actual gas production and model outputs has been achieved. The modeling approach provides a basis for estimating methane inflow and optimizing control measures.

1. INTRODUCTION

Underground longwall mining of coal causes large scale disturbance of the surrounding rock mass. Stress changes and mining induced fracturing of the rock can increase the permeability and can liberate methane from the surrounding strata. The influx of methane can be a significant hazard in longwalling operations and extensive methane mitigation techniques are employed by coal mine operators. However, explosions have been the cause of nine out of eleven coal mining disasters that occurred since 1980 in the USA, [1].

The continued safe extraction of coal by the longwall method requires that methane control methods be both cost effective and reliable. Current methane control methods have been developed largely by field experimentation and trial and error techniques. Nevertheless, on-line monitoring systems are still required that shut down the longwall operations when methane levels exceed a critical value. The difficulty of predicting methane inflow is a significant barrier to designing and optimizing control measures.

Advanced numerical models present an opportunity to realistically simulate rock mass response to longwall operations and the associated methane liberation and flow through the fractured rock mass without resorting to field experimentation. This paper describes the recent application of geomechanical as well as reservoir modeling techniques to investigate the effect of longwall mining on the permeability of the surrounding strata and methane liberation and flow from the surrounding rocks towards the mine workings. The work is largely based on field data and methane

control techniques employed in the coal mines of the Eastern United States.

A two staged approach has been followed to develop models of methane emissions and flow around longwall mines. The first stage has been to make use of the FLAC2D [2] finite difference code to simulate the geomechanical response of the rock mass to longwall mining. The program was used to calculate the stress changes, extent of rock fracturing and bedding plane shear. The output of the FLAC models was used to calculate likely permeability changes, based on empirical relationships. The permeability distribution was then used to develop inputs for the 3-D compositional reservoir simulator (GEM) by Computer Modeling Group [3]. The reservoir simulator was used to develop a model of several longwall panels in a study mine against which the model was calibrated by history matching of gob vent borehole (GVB) methane production. The model has been used to evaluate the relative merits of methane drainage options.

2. PERMEABILITY OF COAL MEASURE ROCKS

Coal measure rocks typically consist of interbedded shale, siltstone, sandstone, claystone and limestone. The permeability is anisotropic because of interlayered low and high permeability strata [4]. Sandstone and limestone beds have the highest permeabilities and act as aquifers, they promote horizontal flow and have relatively high storage capacity. The shales act as aquitards, having low permeability, but may contain fractures and bedding planes that enhance permeability. Thin clay bands can exist within the measures that act as aquicludes. Coal is highly transmissive, but typically has poor storage. The overall permeability of the strata tends to decrease with depth, a decrease of 1 order of magnitude of the permeability of coal for every 25 MPa increase in overburden loading was reported by Sparks [5].

Permeabilities measured in the field can be dominated by fracture flow and are typically highly variable. Tests are usually performed in vertical wells, which provide a better indication of horizontal permeability than vertical. Test results published by Hasenfus et al. [6] in strata above the Pittsburgh coalbed showed that the permeability can vary by several orders of magnitude in different sections of a vertical borehole. They measured

hydraulic conductivities of $7x10^{-6}$cm/s in sandstone near the ground surface. Brutcher et al. [7] tested the conductivity of a sandstone aquifer and found the values to vary between 10^{-4} and 10^{-6} cm/s while shale conductivity was one order of magnitude lower. Booth and Spande [8] reported hydraulic conductivities of $9x10^{-5}$ cm/s for sandstone in Southern Illinois. Matetic et al. [9] reported permeabilities of $7x10^{-6}$ cm/s in shale materials near surface and $7x10^{-5}$ cm/s for sandstone in southeastern Ohio.

The field measured hydraulic conductivities all fall within published ranges for sandstone and shales and the upper limits fall in the range that one would expect for jointed rock. Coal measure rocks in the eastern United States are typically poorly jointed, but contain bedding planes that act as discontinuities which allow horizontal flow. Vertical flow is constrained, especially by thin clay layers.

3. EFFECT OF LONGWALL MINING ON PERMEABILITY

Longwall mining induces both stress increases and stress reductions in the surrounding rock. Around the edges of the panel, the stresses will increase, while the rock directly above and below the extracted panel will experience significant stress relief. In addition, the increased stresses can cause fracturing of the rock mass. These changes can have a profound effect on the rock mass permeability. Field studies have shown both increasing and decreasing changes of approximately one order of magnitude in the hydraulic conductivity of the rock mass above a longwall panel in Pennsylvania [6].

3.1. The effect of stress changes
Changes in stress can produce large variations in the permeability of laboratory and field scale rock. In the laboratory, the permeability will initially decrease as rock is subject to increasing loads, but the permeability will increase as the rock reaches its peak strength, and permeability attains a maximum during the post failure stage [10]. The permeability of the field scale rock mass is affected by the closure or opening of fractures under changing stresses. The equivalent permeability can be related to the fracture aperture and fracture spacing [11, 12, 13]. Some researchers have related changes in permeability directly to changes in the confining

stress, and found an exponential relationship between permeability and stress [14].

3.2. The effect of fracturing

In addition to stress changes, fracturing occurs in the rock mass in the vicinity of a longwall panel. Three zones can be distinguished in the roof rocks, shown in figure 1: the caved zone, fractured zone and the bending zone [15, 16]. The caved zone is created as the mining face advances and the immediate overburden falls and fills the void created by the extraction of the coal. The caved zone extends upwards, 3-6 times the extraction thickness. The caved zone is characterized by irregular rock fragments that may have rotated relative to their initial locations, resulting in relatively high void ratios and permeability. Laboratory tests have shown that the void ratio can be in the order of 30%-45% [17]. As the face advances, the caved rock (gob) is re-compacted by the weight of the overburden. The amount of re-compaction depends on the depth of overburden and the strength of the gob material. The permeability of the caved zone can be expected to be high but will vary as the compaction of the gob varies.
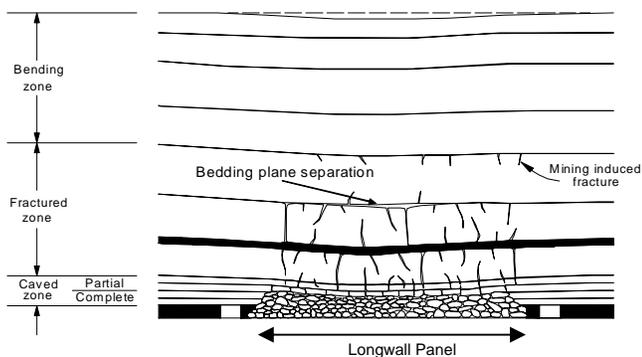

Fig. 1. Schematic vertical section showing strata movement above a longwall panel [16].

The fractured zone is located above and around the caved zone and is characterized by near vertical fractures and bedding plane shearing caused by the passage of the longwall face [6]. Bed separation can occur in this zone. The fractured zone can extend 30 to 60 times the extraction thickness. In this zone, water drains directly to the caved zone and into the mine workings. Measurements of permeability in the fractured rock have shown up to forty fold increases in permeability [18].

Above the fractured zone is the bending zone. The rock is essentially un-fractured, but can experience shearing along bedding planes as they are deflected over the edges of the extracted longwall panel [6]. Bedding plane shear will affect the horizontal conductivity of the rock. Field observations have shown that water levels and ground movements occur up to 60 m (200 ft) ahead of an advancing longwall face. These movements can be associated with shear along weak clay filled bedding planes.

Rock mass disturbance also extends into the floor of a longwall panel. The floor experiences stress relief as the longwall face passes overhead. The stress relief will be partially reversed as the gob is re-compacted by the weight of the overburden. In addition, the elevated abutment stresses can cause deep seated fracturing of the floor rocks at the advancing face and around the stationary abutments. Floor gas emissions are not uncommon in longwall mines and can be explained by the failure and stress relief in the floor.

4. METHANE SOURCES AND CONTROL

The sources of methane in longwall operations are likely to be: the coalbed being mined, overlying or underlying coal coalbeds and to a lesser extent the methane contained within the surrounding rock strata. Porous rocks such as sandstones are likely candidates for gas storage. However, Diamond et al, [19] reported that the primary sources of longwall gob gas resulting from the mining of the lower Kittanning were the coalbeds in the overlying strata. As much as 91% of the longwall gob gas originated in the overlying coalbeds, with those as high as 200 ft above the mined coalbed contributing gas to the gob..

Prior to mining, the gas and groundwater are in equilibrium and are contained by various clay rich layers. The disturbance caused by the longwall mining first dewaters the rock within the caved and fractured zones [4], this is followed by gas liberation mainly from the coalbeds, as the pore pressure drops. The stress relief and mining related fracturing can provide new pathways for the flow of methane to the mined excavations. Material balance calculations indicated that the volume of the gas drained from the strata directly overlying the longwall panel could only account for 40% of the total volume of gas vented by the ventilation system and gob vent boreholes [19]. The rest of the methane migrates from the adjacent formations

towards the low pressure fractured zone. Furthermore, the high permeability caved zone acts as a conduit for methane by providing a connection between the face area and the overlying fractured zone.

Methane control methods can include pre-drainage of methane ahead of the longwall, increased ventilation to dilute the methane, a bleeder ventilation system in which exhaust shafts are dedicated to methane extraction and the extraction of methane from the overburden above a longwall panel through the use of GVB's. Gob vent boreholes are drilled above the panel to capture the gas from subsided and relaxed strata before it enters the mining environment. Most GVB's are drilled within a short distance (10-30 m) of the coalbed being mined and cased with steel pipe. Commonly, the bottom section of the pipe is slotted and placed within the gas production zone, where extensive fracturing occurs as the overburden caves into the unsupported mine void and establishes a preferential pathway for the released gas towards the GVB [20]. Issues such as the optimal location of GVB's relative to the longwall panel edges, and the spacing between GVB's, the correct depth of slotted casing and operational practices have all been based on trial and error methods. Optimal operation of GVB's and the mine ventilation system requires that a balance be found between the pressures and methane flow rates in the GVB system and the bleeder system [21]. Sub-optimal operation of the GVB system will result in excessive methane flow to the workings, while the converse will cause mine air to be drawn towards the GVB's.

5. GEOMECHANICAL MODELING

The geomechanical and reservoir model studies were carried out using data from a study mine in Pennsylvania.

5.1. Geology and Mine Layout
The study mine operates in the Northern Appalachian section of the Pittsburgh Coalbed in Greene County, Southwestern Pennsylvania, USA. In the area, overburden depths ranged between 152 and 274 m (500 and 900 ft). Longwall panels in the primary study area were initially 253 m (830 ft) wide and were increased to 305 m (1,000 ft). The panels are super critical, i.e. caving and subsidence of the overburden is fully developed, and an

increase in the panel width does not result in an increase in the maximum surface subsidence.

A generalized stratigraphic section of the strata above the Pittsburgh Coalbed in the study area is shown in Figure 2. Several coalbeds with a combined thickness of almost 3 m (10 ft) are present in the 26 m (85 ft) of strata immediately above the Pittsburgh Coalbed, and thought to be the primary source of strata gas in the area. Within this interval, the thickest coalbed is the Sewickley Coalbed, which is about 25 m (75 ft) above the Pittsburgh coalbed and the Waynesburg coalbed about 70 m (230 ft) above the Sewickley. Also important from a geomechanical point of view is the presence of substantial limestone beds in the roof of the Pittsburgh coalbed. The limestone is stiffer and stronger than the surrounding shale, claystone and siltstone rocks.
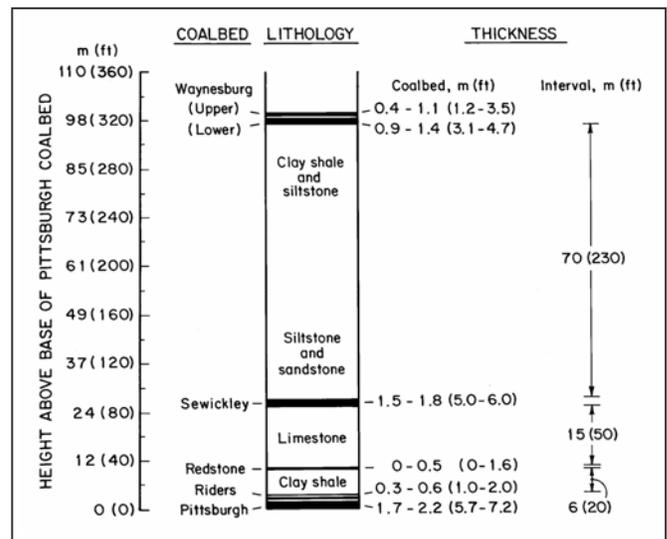

Figure 2: General stratigraphy at case study mine, showing variation various rock types incorporated in FLAC model.

5.2. Model Geometry and Mining Sequence
FLAC 2D models were used to simulate rock behavior along a longitudinal section through the center line and a section across the width of a typical longwall panel at the study mine. The longitudinal sections were used to assess stress changes and rock failure around the advancing longwall face. The cross section was used to assess rock behavior around the edges of the longwall, which included the behavior over the chain pillars that are left between longwalls.

The model dimensions were typically 400 m (1,300 ft) wide by 350 m (1,150 ft) deep to simulate a longitudinal section through a longwall panel.

The models included the ground surface, the Pittsburgh Coalbed at 180 – 200 m (600 - 650 ft) below the surface and the surrounding roof and floor rocks. Element sizes varied, but were selected so that the element size was 1 m in the zone of interest, near the longwall face. Element sizes increase with increasing distance form the area of interest. Figure 3 shows the general layout of a FLAC grid indicating the main rock types.
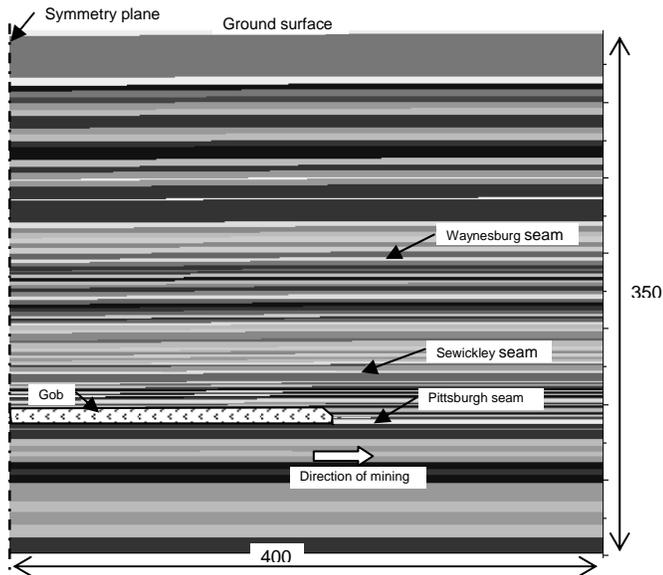

Fig. 3. Longitudinal FLAC model showing layering in the model, the location of the main seams and the gob behind the advancing longwall face.

Mining was simulated in increments, starting from the left side of the grid and advancing to the right. Extraction of the coalbed was modeled by removing elements over the height of the coalbed by 2 elements wide. The process of gob formation was modeled by first deleting rock elements in the roof of the coalbed, so that they are stress relieved, followed by inserting gob properties in these elements. Gob properties were also inserted in previously mined coalbed elements, so that the gob filled the mined void. A 2 m (6.5 ft) opening was maintained between the face and the gob, to represent the working area. The height of the gob was four times the mining height.

The model was run to equilibrium at each step, so that rock failure and stress re-distribution would occur. The model included sufficient lateral extent of mining so that full subsidence of the overburden strata would occur over the mined area, representing super critical conditions.

5.3. Rock Mass and Gob Parameters

The rock mass was modeled as a strain softening/ubiquitous joint material, using the built-in constitutive model in FLAC. This model is well suited to modeling the layered coal measure rocks, since the bedding layers can be described as ubiquitous joints, while failure of the rock matrix can be simulated as a strain softening Coulomb material. Great care was taken in setting up the models to replicate the geological sequence with as much detail as practical.

Strength data for the different rock types included in the models were obtained from laboratory tests [22] as well as field index testing using the point-load apparatus on core from the test mine. The mean and standard deviation of the intact strength as well as the bedding strength was determined for each rock type. A random sampling technique was then used to apply rock strengths to different layers in the FLAC models, each layer corresponding to a section of a logged core hole.

Table 1 presents the key strength data used in the models. The strain softening parameters were the same for all the rock types. Cohesion softening was assumed, with a 90% drop in cohesion after 5.0 millistrain of inelastic deformation. The friction

Table 1. Mechanical Properties of Rock Strata used in Models

Rock class	Rock types	Cohesion (MPa)	Friction Angle	Poisson Ratio	Elastic Modulus (GPa)
Stiff soil	Clay bands	0.055	21	0.25	1.5
Very weak rock	Very weak rock, claystone, drawslate	2.0	23	0.25	4.0
Weak rock	Weak rock, Black carbonaceous shale	4.5	25	0.25	6.0
Moderate rock	Moderate rock, Shale,	8.0	28	0.25	8.0
Strong rock	Sandstone	12.0	32	0.25	12.0
Very strong rock	Limestone	20.0	36	0.25	20.0
Coal	Coal	1.9	31	0.25	2.5

angle remained unchanged after failure. The dilation angle was assumed to be 10º initially decreasing linearly to zero after 5.0 millistrain. The tensile strength was set at one tenth the compressive strength, decreasing to zero after 1.0 millistrain. Table 2 shows the properties used for bedding planes. Bedding properties were defined independently of the rock type since strong rocks can have weak bedding planes. The bedding properties were also assigned on a layer by layer basis in the models.

The gob was modeled as a double-yield material which is a constitutive model in FLAC that can model the compaction of granular materials. Inputs for the gob material were determined through a trail and error approach by first matching the modeled behavior to the results of laboratory tests on simulated gob material, [17]. This was followed by further modifying the parameters so that the surface subsidence above the longwall panels in the models matched observed subsidence. The final set of inputs used for the gob material were as follows: Bulk modulus = 0.45 GPa, Shear modulus = 0.60 GPa and Friction angle = 40°. The stress-strain characteristics of the gob is defined by the "cap pressure" table given in Table 3.

5.4. Stress and Boundary Conditions

The initial field stresses in the models were based on the approach that the rock mass is subject to a constant horizontal strain as a result of plate tectonics, [23]. A review of stress measurements in the Eastern United States [24] showed that the elastic modulus of the rocks is the main factor controlling the horizontal stress. For the Northern Appalachian region, the maximum horizontal stress in a rock layer can be determined by its laboratory scale elastic modulus and assuming a constant horizontal strain of about 0.5 millistrain. The tectonic stress is additional to horizontal stress caused by the Poisson effect of gravity loading. For the purpose of modeling, the vertical stress was assumed to be directly dependent on the cover load, the maximum horizontal stress was computed from the constant strain model, and the minor horizontal stress was assumed to be equal to the vertical stress. As a result of the dependence of horizontal stress on the elastic properties of the rock, the initial stress state was initialized within each rock layer individually.

Model boundaries were selected so that they would be sufficiently far from the mining area that they would only have a negligible effect on the results.

Table 2. Properties of Bedding Planes used in Models

Bedding Plane Description	Cohesion (MPa)	Friction angle
Very weak – clay fill	0.055	21
Weak – open joint	0.5	21
Moderate – weakly healed	3.3	24
Strong – healed bedding plane	5.5	26
Very strong – strongly healed bedding plane	10.0	28

Table 3. Cap pressure table for double yield gob elements

Strain	0.0	0.02	0.05	0.07	0.1	0.12	0.15	0.17	0.20
Pressure (MPa)	0.0	0.1	0.3	0.6	1.25	2.25	5.00	10.00	20.00

Table 4. Rock mass permeabilities (and hydraulic conductivities) used in models

Rock Class	Rock types	Horizontal permeability (md)	Horizontal conductivity (cm/s)	Vertical permeability (md)	Vertical permeability (cm/s)
Soil	Clay bands	0.1	9.66×10^{-8}	0.1	9.66×10^{-8}
Very low permeability	Black Shale	0.2	1.93×10^{-7}	0.1	9.66×10^{-8}
Low permeability	Gray shale	1.0	9.66×10^{-7}	0.5	4.83×10^{-7}
Coal - face cleat direction	Coal	4.0	3.86×10^{-6}	0.1	9.66×10^{-8}
Coal – butt cleat direction	Coal	1.0	9.66×10^{-7}	0.1	9.66×10^{-8}
Moderate permeability	Limestone	2.0	1.93×10^{-6}	2.0	1.93×10^{-6}
High permeability	Sandstone	10	9.66×10^{-6}	10	9.66×10^{-6}

The displacements were fixed along the bottom and right sides of the models, while the ground surface was modeled as a free surface. The left boundary was modeled as a symmetry plane.

5.5. Rock Permeability and Calculation of Permeability Changes

Initial permeabilities in the rock mass were based on field scale data from mines in the Eastern United States, discussed earlier, as well as other published sources [4, 12, 25, 26]. Table 4 summarizes the horizontal and vertical permeabilites used in the models.

Permeability changes were calculated for both stress changes and rock fracturing. An exponential relationship was used to compute the effect of stress changes on rock mass permeability after the work of Ren & Edwards [27] and Lowndes et al. [14]. Permeabilities were calculated independently for the horizontal and vertical directions. The parameters were set so that a stress change of 10 MPa would result in a change in permeability of about one order of magnitude. The following equations were used to determine the stress affected horizontal and vertical permeabilites respectively:

$$K_h = K_{h0} \times e^{-0.25(\sigma_{yy} - \sigma_{yy0})}$$

$$K_v = K_{v0} \times e^{-0.25(\sigma_{xx} - \sigma_{xx0})}$$

where σ_{xx} and σ_{yy} are the horizontal and vertical stresses and the 0 subscript indicates initial conditions.

The permeability of fractured rock was determined from published values of jointed rock and fractured rocks [12]. Model elements that fail in compression are assumed to experience an increase in permeability of 100 millidarcy (md) above their current permeability in both the horizontal and vertical directions, regardless of rock type. Similarly bedding shear failure is assumed to increase the permeability by 50 md in the bedding (horizontal) direction. The fracture and shear related permeability changes are added to the current permeabilities at the time of failure. The new permeability is then subject to further variation as a result of stress changes using logic described above.

The built-in programming language in the FLAC model was used to develop a simple algorithim that uses the initial and current stresses as well as the failure state of the rock mass to calculate the permeability at every element. The equations were set up to calculate both the horizontal and vertical permeability. These values formed the basis for the permeability input to the reservoir model. Since the reservoir model was based on larger element sizes than those used in the FLAC model, the resultant permeabilities were averaged over corresponding areas to provide input to the reservoir model.

5.6. Results of FLAC analyses

The results of a FLAC model, showing the fracturing and horizontal permeability distribution about an advancing longwall face are shown in Figure 4. The distinct effect of mining related fracturing on permeability can be seen. It can be seen that the limestone below the Sewickley coalbed is relatively un-fractured by the mining. The fractured zone can be seen to be strongly developed above the gob and below this limestone layer. However, above the limestone the fracture zone is not contiguous, but appears to be confined to shearing along bedding planes in the weaker beds. Bedding shear can be seen to take place up to and above the Waynesburg coalbed. Although not shown in this plot, bedding shear occurs in weak beds above those shown in the figure. Figure 4 also shows the typical location of a GVB, being approximately 12 m (40 ft) above the mined coalbed. It can be seen that the GVB is well within the fractured zone where permeabilities are in the order of 50-100 md. In addition, the stresses are reduced in this area, resulting in an approximately two to five fold increase in permeability of the unfractured rock. The GVB would be well connected to any gas emanating from the Sewickley coalbed. It is also well connected to the highly permeable gob.

Figure 5 shows a cross section across a longwall panel. Here the rock fracture, shearing and permeability distribution around a chain pillar is shown. It can be seen that the high stresses around the pillar create a low permeability zone. Rock fracturing creates high permeability areas around the edges of the pillar, and particularly down into the floor rocks. The strong limestone below the Sewickley coalbed acts as an inhibitor of the fracturing in the roof rocks, however, owing to reduced stresses, the vertical permeability in the limestone increases by a factor of about 2.0. A zone of lower permeability can be seen in and around the two chain pillars, with higher permeability around the entry between the pillars. A higher permeability

zone exists in the roof above the gob on either side of the chain pillars where permeability changes are similar to those seen in Figure 4. The gob vent holes are usually targeted into this zone. It can be seen that the GVB would be well positioned to collect gas from the Sewickley coalbed.
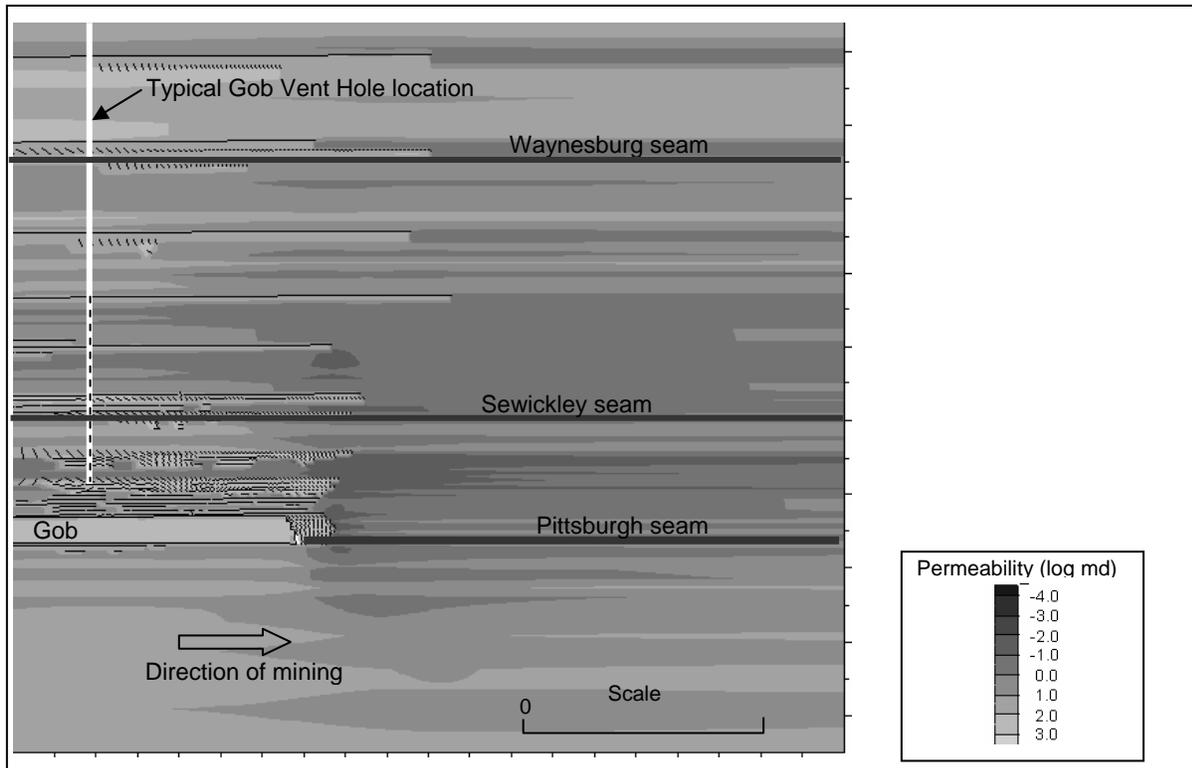

Fig. 4. FLAC model results of a vertical longitudinal-section through an advancing longwall face showing horizontal permeability contours, rock fracturing and bedding plane shear.
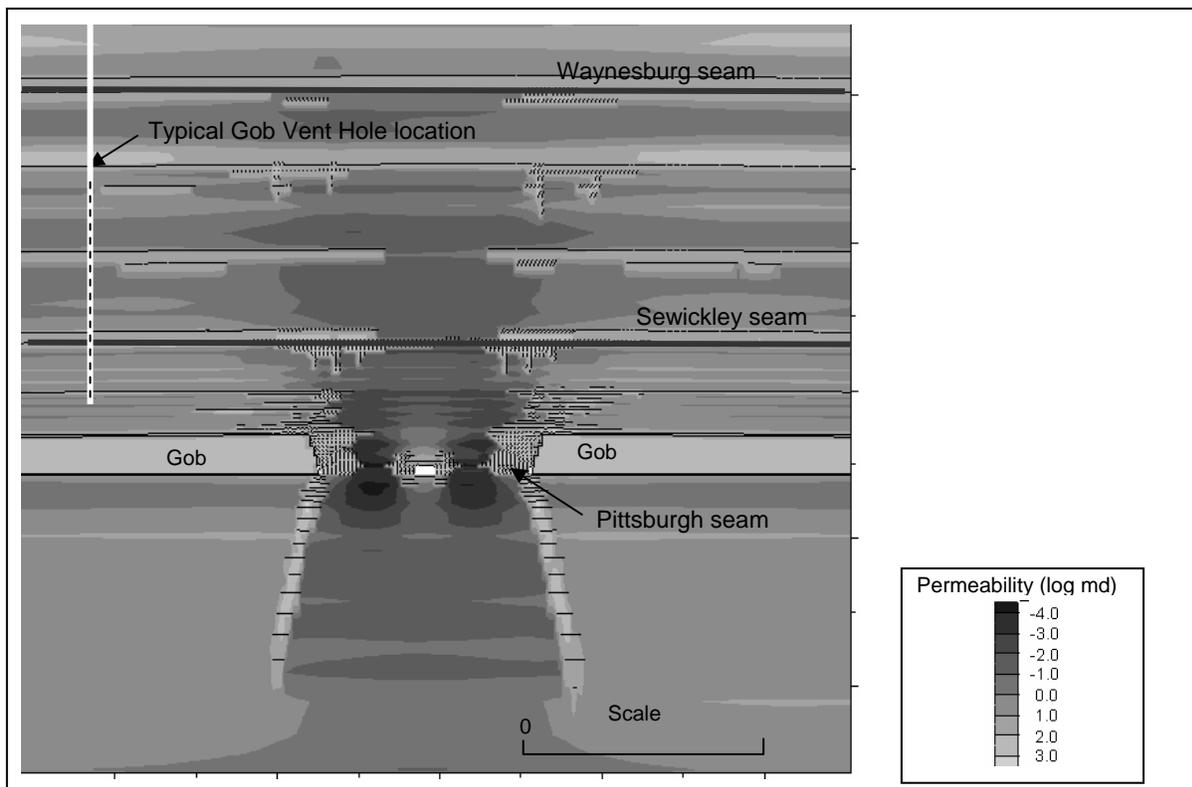

Fig. 5. FLAC model results of a vertical cross-section through a chain pillar between two longwall panels showing horizontal permeability contours, rock fracturing and bedding plane shear.

6. APPLICATION OF RESERVOIR MODEL

6.1. Model Layout and Simulation Execution

The reservoir model was constructed using Computer Modeling Group's [3] compositional reservoir simulator, GEM, which is an efficient, multidimensional, equation-of-state (EOS) compositional simulator that can simulate the dual-porosity behavior of coalbeds for coalbed/enhanced coalbed methane recovery. The dual-porosity approach is the most widely used technique for coal and coal-rock composite reservoirs [28, 29, 30]. In this formulation, fracture-fracture, and matrix-fracture transfers are allowed. In order to handle fluid compositions and sorption/desorption time delays, compositional non-equilibrium models are generally used for coal layers. A detailed description of the reservoir modeling approach is presented in Karacan et al. [31]

Figure 6 shows the 3-D grid model that was constructed of the study mine. In the grid model, the top-most layer of the model was assigned as the Waynesburg Coalbed, and the bottom-most layer was dedicated to the Pittsburgh Coalbed, or mining layer. The other lithologies were represented in the grid model based on their thicknesses and sequences as a function of depth. For convenience in generating the grids, the layers were assumed to be uniform in thickness and continuous throughout the field. The number of vertical layers and their thicknesses were based on the generalized stratigraphy of the area.

In the model, the locations of GVB's were determined based on their locations on the panels. Their completions were modeled based on their actual completion data. At this mine site the GVB's were drilled to within 12-13 m (40-45 ft) of the top of the Pittsburgh Coalbed, and the 17.8-cm (7-in) casing, with 61 m (200 ft) of slotted pipe on the bottom, was installed.

Restart models were constructed to model the advancing longwall as a moving boundary problem. These models were run sequentially, each characterizing a mining stage and its related strata disturbance. In this process, the simulation outputs from the previous model were written in a "restart" file, the next model used this file as the initial condition and updated the longwall face and reservoir changes due to the geomechanical disturbance resulting from the next face position. At this stage, the averaged permeabilities calculated by
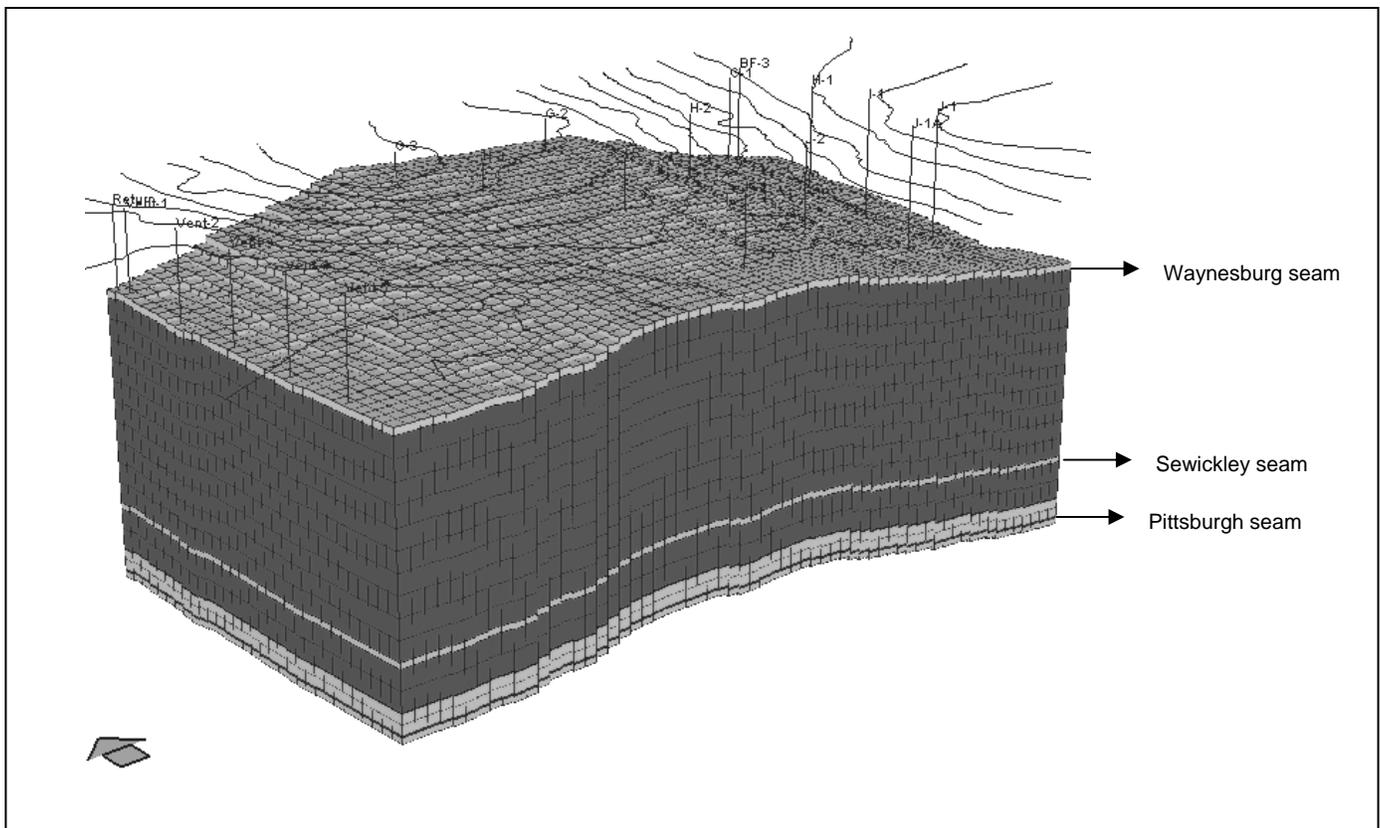

Fig. 6. The 3-D grid model representing the stratigraphic section on the right and the locations of GVB's.

the FLAC models were incorporated into the model to simulate fracturing of the strata and permeability changes due to mining.

6.2. *Example of Results/Calibration*

Model calibration was performed through history matching of the model outputs to the observed production of the gob wells. In this study mainly, disturbed/undisturbed permeability values, a coal desorption time constant, and the permeability of the caved zone were used for matching the gas flow rates and gas compositions from gob gas ventholes. Then, the simulated gas rate and concentrations from each GVB were compared with the actual data. Based on the comparison between simulated and actual productions for the entire period of simulation, adjustments were made to the unknown parameters, and additional runs were completed until an acceptable agreement was judged to be made. During the history match runs, while adjustments were being made to the unknowns, GVB's were operated with the targeted gas rates that were the observed daily rates given on weekly basis as the well control constraint, and wellbore pressures were computed by the simulator. However, the acceptance criteria for the calculated pressures were that they should be lower than and close to atmospheric pressures, as they normally should be in the field [32]. Further verification of the model output was carried out by comparing the methane concentrations from the GVB's, calculated by the simulator, to the field measurements.

Figure 7 shows the actual and simulated gas production rates for a total of four wells (one well from each panel in a four panel area) from the calibrated model. As can be seen from this figure, the rate data matches satisfactorily for most of the data points using the applied methodology. The actual and simulated methane concentrations from one well in each panel are presented in Figure 8. This shows that the methane concentrations can be matched for average values and general trends. Figure 9 shows the bottom hole pressures for the four wells, indicating that the pressures remain at or near atmospheric values after the well was intercepted and became operational, as observed in the field. This approach has been successful for calibration of the model and gives some degree of confidence to the predictive capability of the model developed.

The reservoir simulator was used to study the source of longwall gas over the study mine. Figure 10 shows a slab that represents the vertical section of the reservoir over one of the panels after the 630th day since the start of mining and presents the methane concentration in the strata at that stage. The results indicate a high concentration of methane below the Waynesburg coalbed, but the flow rate in this area is low owing to absence of extensive fracturing. Closer to the mined coalbed the gas flow rate is higher and the gas tends to flow towards the GVB's if they are in operation. The figure shows two GVBs and their effect in reducing methane concentrations below the Sewickley at that specific time.

7. SUMMARY AND CONCLUSIONS

The study has shown that the two stage approach, which combines the output of geomechanical models with reservoir models, is capable of realistically simulating the complex process of methane emission and flow around longwall panels in coal mines.

The FLAC geomechanical models provide valuable insight into the permeability distributions around a longwall panel. The effect of rock fracturing as well as stress changes on permeability can be directly modeled. The permeability plots show that the typical GVB positions are well located to intersect the higher permeability zones above the gob. The reservoir model has been successful in matching actual gob gas production at the study mine, and can be used to evaluate methane sources and flow patterns in the overburden. The model showed that the GVB's were effective in capturing gas from the overlying Sewickley coalbed at the study mine.

The modeling approach provides a basis for evaluating methane inflow and control measures. This approach will result in increased safety for mine workers in longwall mines by improving our ability to predict methane inflows and enabling more effective design of methane control measures.
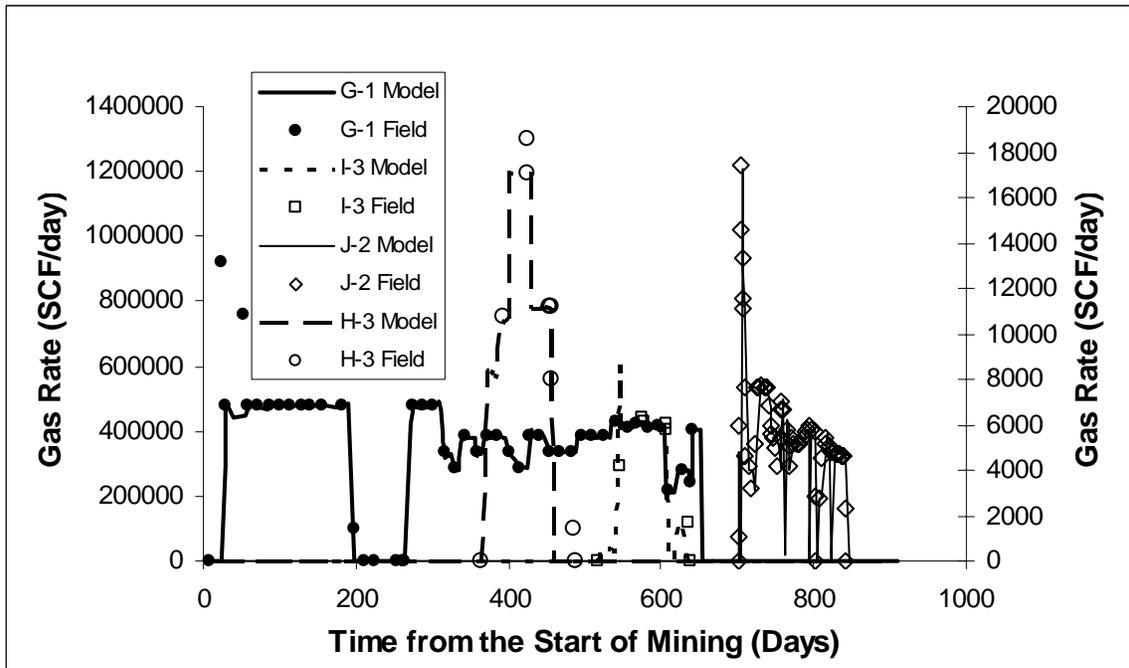
Fig. 7. Comparison of observed and simulated gas production rates from one GVB at each panel.
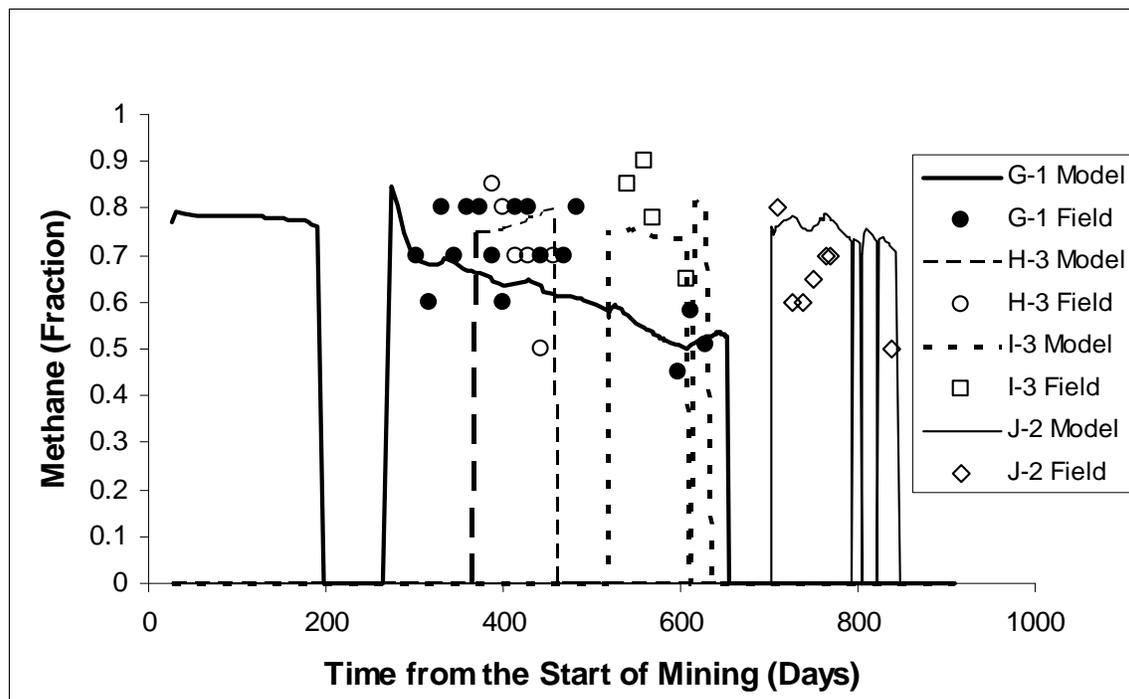

Fig. 8. The comparison of observed and simulated methane concentrations from one GVB at each panel mined based on current longwall mining modeling approach.
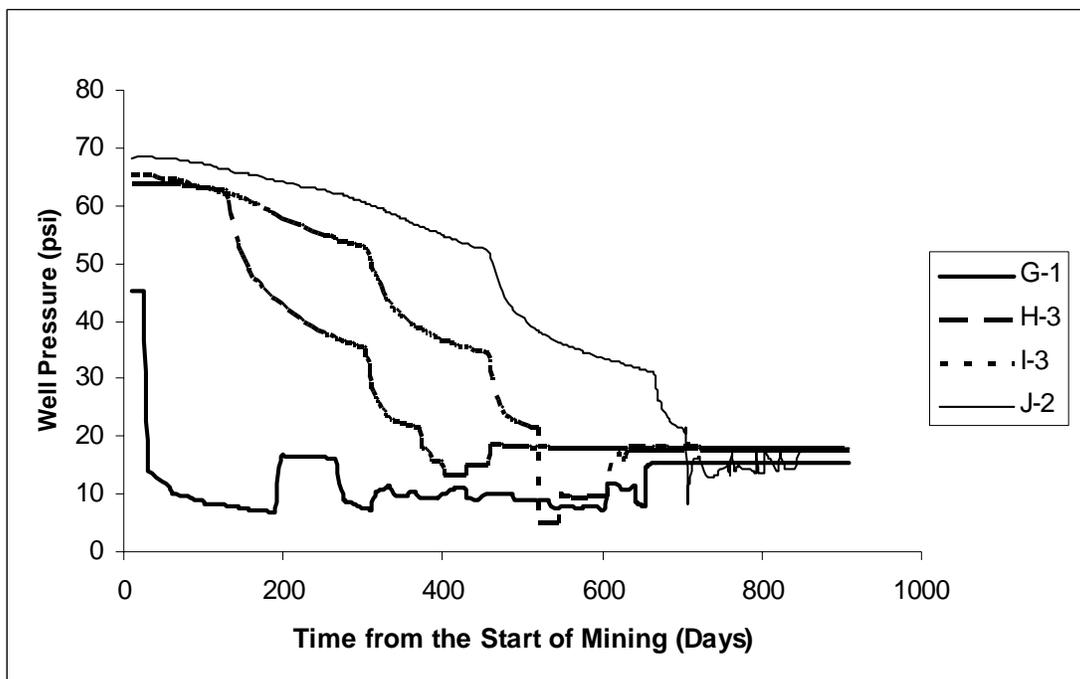
Fig. 9. The bottom hole pressures calculated by the model for the shown GVBs of each panel.
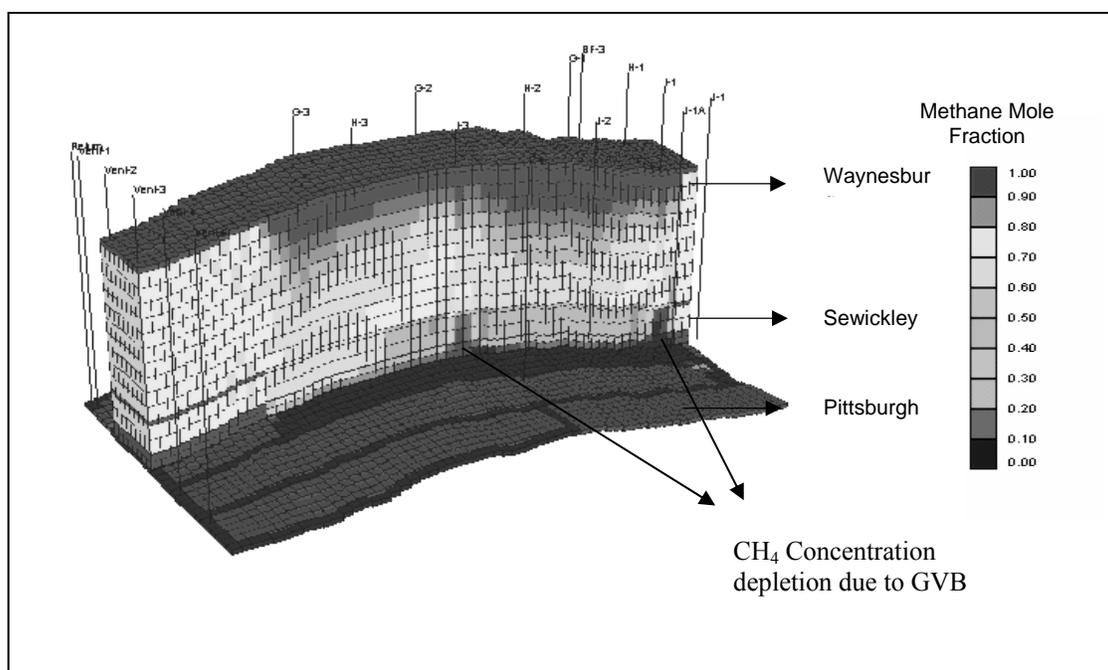

Fig. 10: A slab that shows the vertical section of the reservoir over headgate side of a panel and the Pittsburgh Coalbed layer after 630th day since the start of mining. Figure shows the methane emissions (as mole fraction) and two of the operating GVB's

REFERENCES

1. NIOSH. National Institute for Occupational Safety and Health, web page: http://www.cdc.gov/ niosh/ mining/ topics/ data/ tables/ discoal.html

2. Itasca Consulting Group. 2000. Fast Lagrangian analysis of continua. *2nd Edition, Minnesota*.

3. Computer Modeling Group Ltd. 2003. Generalized equation of state model-GEM, *User's Guide, Calgary, Alberta, Canada*.

4. Booth, C.J. 1984. A numerical model of groundwater flow associated with an underground coal mine in the Appalachian plateau, Pennsylvania. *PhD Thesis*, University of Pennsylvania.

5. Sparks, D.P. 1993. Coalbed gas well flow performance controls, Cedar Grove Area, Warrior Basin, USA. *International Coalbed Methane Symposium, University of Alabama, Tuscaloosa II*: 529-548.

6. Hasenfus, G.J., K.L. Johnson and D.H.W. Su. 1988. A hydrogeomechanical study of overburden aquifer response to longwall mining. In *Proceeding of the 7th Int. Conf. Ground Control in Mining,* 149-162.

7. Brutcher, D.F., B.B. Mehnert, D.J. van Roosendal and R.A. Bauer. 1990. Rock strength and overburden changes due to subsidence over a longwall coal mining operation in Illinois. *Rock Mechanics Contributions and Challenges, 31st US Symposium on Rock Mechanics, Golden Colorado,* 563-570.

8. Booth, C.J. and E.D. Spande. 1992. Potentiometric and aquifer property changes above subsiding longwall mine panels, Illinois basin coalfield. *Ground Water 30: 2,* 362-368.

9. Matetic, R.J., J. Liu and D. Elsworth. 1995. Using Multiple-point borehole extensometers and finite element modeling in coordination with hydrologic field data to determine post-mining effects to the ground water system. *Outdoor Action Conference, National Ground Water Association, Las Vegas, NV, 2 - 9 May 1995.*

10. Wang, J.A. and H.D. Park. 2002. Fluid permeability of sedimentary rocks in a complete stress-strain process. *Engineering Geology 63*: 291-300.

11. Bai, M. and D. Elsworth. 1993. Influence of mining geometry on mine hydro-geo-mechanics. *SME Annual Meeting, Reno, Nevada*, Preprint 93-6.

12. Hoek, E. and J.W. Bray. 1981. Rock slope engineering. *3rd edition, Inst. Min. Metall. London.*

13. Louis, C. 1969. A study of groundwater flow in jointed rock and its influence on the stability of rock masses. *PhD thesis, Univ. Karlsruhe.*

14. Lowndes, I.S., D.J. Reddish, T.X. Ren, D.N. Whittles, and D.M. Hargreaves. 2002. Improved modeling to support the prediction of gas migration and emission from active longwall panels. *Mine Ventilation*. eds. Euler De Souza, Balkema, 267-272.

15. Peng, S.S.. 1984. Longwall Mining, Wiley, New York.

16. Singh, M.M. and F.S. Kendorski. 1981. Strata disturbance prediction for mining beneath surface water and waste impoundments. *1st Conf. Ground Control in Mining, Morgantown, WV*, 76-89.

17. Pappas, D.M. and C. Mark.. 1993. Behavior of simulated gob material. *U.S. Bureau of Mines Report of Investigations RI 9458.*

18. Whittaker, B.N., R.N. Singh and C.J. Neate. 1979. Effect of longwall mining on ground permeability and subsurface drainage. In *Proceedings of the First International Mine Drainage Symposium*, 161-183.

19. Diamond, W.P., J.P. Ulery, and S. J. Kravitz,. 1992. Determining the source of longwall gob gas: Lower Kittanning Coalbed, Cambria County, PA. *Bureau of Mines, Information Circular No: 9430.*

20. Diamond, W.P. 1994. Methane Control for Underground Coal Mines. *U.S. Bureau of Mines, Information Circular 9395.*

21. Mucho, T. 2004. Personal communication.

22. Rusnak, J.A. and C. Mark. 1999. Using the point load test to determine the uniaxial compressive strength of coal measure rock. In *Proceeding of the 19th Int. Conference on Ground Control in Mining*, 362-371.

23. Mark, C. and T.P. Mucho. 1994. Longwall mine design for the control of high horizontal stress. In *Proceeding of the New Technology for Longwall Ground Control, US Bureau of Mines, Special Publication 01-94*, 53-76.

24. Dolinar, D.R. 2003. Variation of horizontal stresses and strains in mines in bedded deposits in the eastern and midwestern United States. In *Proceeding of the 22nd Int Conf. Ground Control in Mining, Morgantown, West Virginia,* 178-185.

25. Franklin J.A. and M.B. Dusseault. 1989. *Rock Engineering*, McGraw-Hill.

26. Leedan, Van der F., F.L. Troise and D.K. Todd. 1991. *The Water Encyclopedia.* 2nd edition, Lewis, Michigan.

27. Ren, T.X. and J.S. Edwards. 2002. Goaf gas modeling techniques to maximize methane capture from surface gob wells. *Mine Ventilation*: 279-286.

28. Ertekin, T., W. Sung, and F.C. Schwerer. 1988. Production performance analysis of horizontal drainage wells for the degasification of coal seams. *Journal of Petroleum Technology*, May, 625-631.

29. King, G. and Ertekin, T. 1991. State of the Art Modeling for Unconventional Gas Recovery, SPE Formation Evaluation, March, pp. 63-72.

30. Young, G.B.C., G.W. Paul, J.L. Saulsberry, and R.A. Schraufnagel. 1993. A simulation-based analysis of multiseam coalbed well completions, SPE Paper 26628, In *Proceedings of the 68th Society of Petroleum Engineers Annual Technical Conference and Exhibition,* 205-215.

31. Karacan, C.O., G.S. Esterhuizen, S. Schatzel, and W.P. Diamond. 2005. Reservoir simulation-based modeling for characterizing longwall methane emissions and gob gas venthole production. *Int J. Coal Geology* (to be published).

32. Garcia F. Personal communication, 2003.